ACS APPLIED MATERIALS & INTERFACES

Research Article

www.acsami.org

Naphthalene-, Anthracene-, and Pyrene-Substituted Fullerene Derivatives as Electron Acceptors in Polymer-based Solar Cells

Hee Un Kim,[†] Ji-Hoon Kim,[†] Hyunbum Kang,[‡] Andrew C. Grimsdale,[§] Bumjoon J. Kim,[‡] Sung Cheol Yoon,[∥] and Do-Hoon Hwang*[,†]

[†]Department of Chemistry and Chemistry Institute for Functional Materials, Pusan National University, Busan 609-735, Republic of Korea

[‡]Department of Chemical & Biomolecular Engineering, Korea Advanced Institute of Science and Technology (KAIST), Daejeon 305-701, Republic of Korea

[§]School of Materials Science and Engineering, Nanyang Technological University, 50 Nanyang Avenue, Singapore 639798

[∥]Advanced Materials Division, Korea Research Institute of Chemical Technology (KRICT), Daejeon 305-600, Republic of Korea

Supporting Information

ABSTRACT: A series of aryl-substituted fullerene derivatives were prepared in which the aromatic moiety of [6,6]-phenyl C_{61}-butyric acid methyl ester ($PC_{61}BM$) was modified by replacing the monocyclic phenyl ring with bicyclic naphthalene ($NC_{61}BM$), tricyclic anthracene ($AC_{61}BM$), and tetracyclic pyrene ($PyC_{61}BM$). The $PC_{61}BM$ derivatives were synthesized from C_{60} using tosylhydrazone and were tested as electron acceptors in poly(3-hexylthiophene) (P3HT)-based organic photovoltaic cells (OPVs). The lowest unoccupied molecular orbital (LUMO) energy level of $NC_{61}BM$ (−3.68 eV) was found to be slightly higher than those of $PC_{61}BM$ (−3.70 eV), $AC_{61}BM$ (−3.75 eV), and $PyC_{61}BM$ (−3.72 eV). The electron mobility values obtained for the P3HT:$PC_{61}BM$, P3HT:$NC_{61}BM$, P3HT:$AC_{61}BM$, and P3HT:$PyC_{61}BM$ blend films were 2.39×10^{-4}, 2.27×10^{-4}, 1.75×10^{-4}, and 2.13×10^{-4} $cm^2\ V^{-1}\ s^{-1}$, respectively. P3HT-based bulk-heterojunction (BHJ) solar cells were fabricated using $NC_{61}BM$, $AC_{61}BM$, and $PyC_{61}BM$ as electron acceptors, and their performances were compared with that of the device fabricated using $PC_{61}BM$. The highest power conversion efficiencies (PCEs) observed for devices fabricated with $PC_{61}BM$, $NC_{61}BM$, $AC_{61}BM$, and $PyC_{61}BM$ were 3.80, 4.09, 1.14, and 1.95%, respectively, suggesting $NC_{61}BM$ as a promising electron acceptor for OPVs.

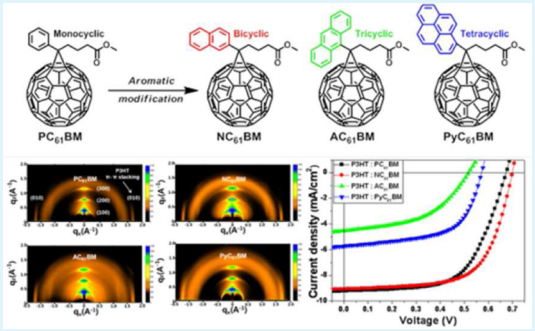

KEYWORDS: *fullerene (C_{60}) derivative, electron acceptor, organic photovoltaic cell (OPV), bulk-heterojunction*

INTRODUCTION

The demand for inexpensive, renewable energy sources continues to stimulate new approaches to the production of efficient, low-cost organic photovoltaic cells (OPVs).[1−5] OPVs based on bulk-heterojunctions (BHJs) use a phase-separated blend of electron-donating polymers such as poly(3-hexylthiophene) (P3HT) and electron-accepting materials such as [6,6]-phenyl-C_{61}-butyric acid methyl ester ($PC_{61}BM$).[6,7] Since the earliest reports of BHJ OPVs, fullerene derivatives have been used almost exclusively as acceptors in OPVs fabrication.[8−10] This is due to the exceptionally rapid rate at which they accept electrons from conjugated donor polymers, combined with the slow rate at which the reverse electron transfer occurs and the excellent electron transport properties they exhibit.[11−13] Recently, a rich variety of fullerene-based electron acceptors have been developed for potential use in BHJ solar cells. Various modifications to C_{60} fullerenes have been studied for improving solubility, controlling the lowest unoccupied molecular orbital (LUMO) energy level, and enhancing the light-harvesting ability.[14−27]

$PC_{61}BM$, in particular, has become one of the most widely used electron acceptors and has been extensively studied because of its good solubility characteristics and the high power conversion efficiency (PCE) it exhibits in OPVs devices. Research on $PC_{61}BM$ most often involves structural modification of the aromatic phenyl and aliphatic butyric methyl ester moieties. For example, Troshin et al. reported on the synthesis and photovoltaic properties of various $PC_{61}BM$ derivatives by replacing the phenyl group with alkoxyphenyl, thiophenyl, and furanyl moieties; additionally, they further altered the molecule by changing the alkyl spacer length, or the alcohol part of the ester, and by replacing the ester functionality with a ketone.[15] Because most of the synthesized derivatives exhibited lower or at best comparable PCE in P3HT-based photovoltaic cells when compared with unmodified $PC_{61}BM$,

Received: July 28, 2014
Accepted: November 13, 2014
Published: November 13, 2014

Scheme 1. Synthesis and Chemical Structures of $NC_{61}BM$, $AC_{61}BM$, and $PyC_{61}BM$

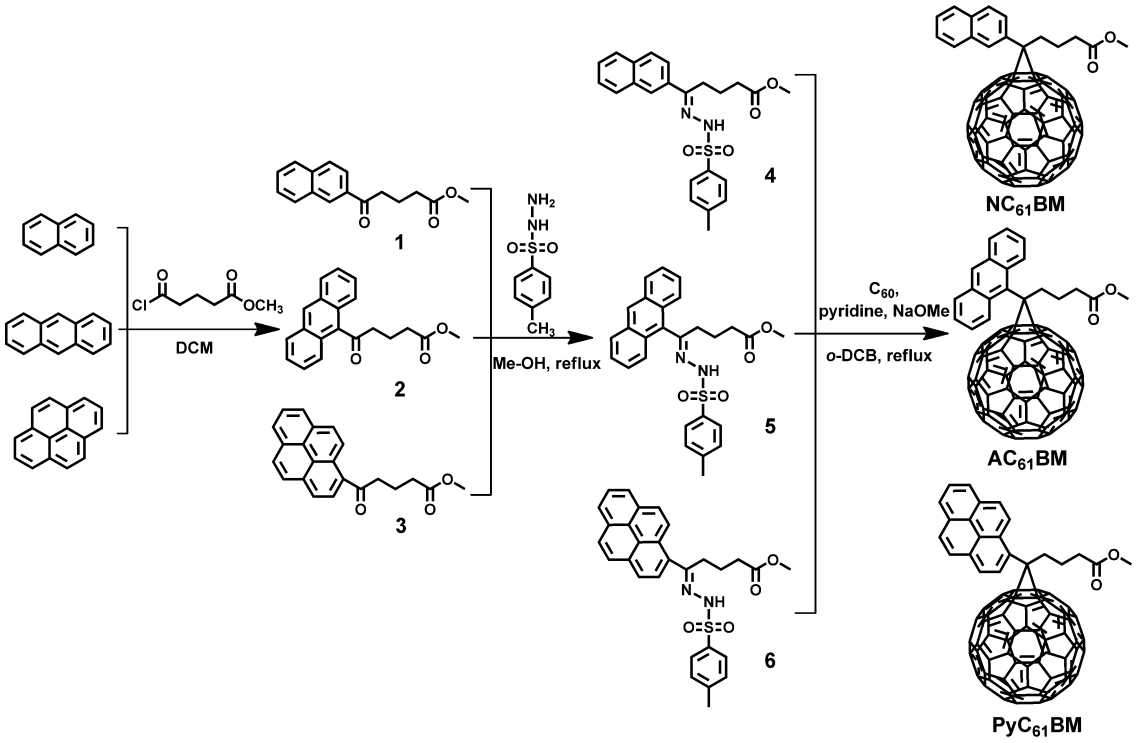

there remains a need to produce derivatives that show higher performance.

In this study, we investigate the effects of changing the $PC_{61}BM$ aryl group on photovoltaic performance. We replaced the phenyl ring with naphthalene (bicyclic), anthracene (tricyclic), and pyrene (tetracyclic) and investigated the photophysical properties of the resulting $NC_{61}BM$, $AC_{61}BM$, and $PyC_{61}BM$. The synthesis and chemical structures of these aryl-substituted fullerene derivatives are shown in Scheme 1.

RESULTS AND DISCUSSION

Synthesis and Characterization. $NC_{61}BM$, $AC_{61}BM$, and $PyC_{61}BM$ were synthesized by reacting the appropriate aryl tosylhydrazone with C_{60}, as shown in Scheme 1; this reaction is known to proceed through a carbene intermediate.[6] The synthesized fullerene derivative formation was confirmed by ^{1}H and ^{13}C NMR, as well as by fast atom bombardment mass spectroscopy (FAB-MS; Figures S1 and S2 in the Supporting Information). All the synthesized fullerene derivatives showed good solubility in common organic solvents such as chloroform, toluene, and 1,2-dichlorobenzene.

The thermal properties of both $PC_{61}BM$ and the new aryl-substituted fullerene derivatives were investigated by thermogravimetric analysis (TGA). The 5% weight loss temperatures (T_d) for $PC_{61}BM$, $NC_{61}BM$, $AC_{61}BM$, and $PyC_{61}BM$ were measured to be 402, 420, 443, and 487 °C, respectively (Figure S3, Supporting Information), indicating that the synthesized aryl-substituted fullerene derivatives were more thermally stable than $PC_{61}BM$. Overall, T_d values increased with the substituent size increased.

Optical Properties. Figure 1a shows the UV−visible absorption spectra measured for $PC_{61}BM$ and the new aryl-substituted fullerene derivatives in 1,2-dichlorobenzene solution (10^{-5} M). The synthesized derivatives showed a similar absorption band in the range of 330−400 nm and exhibited

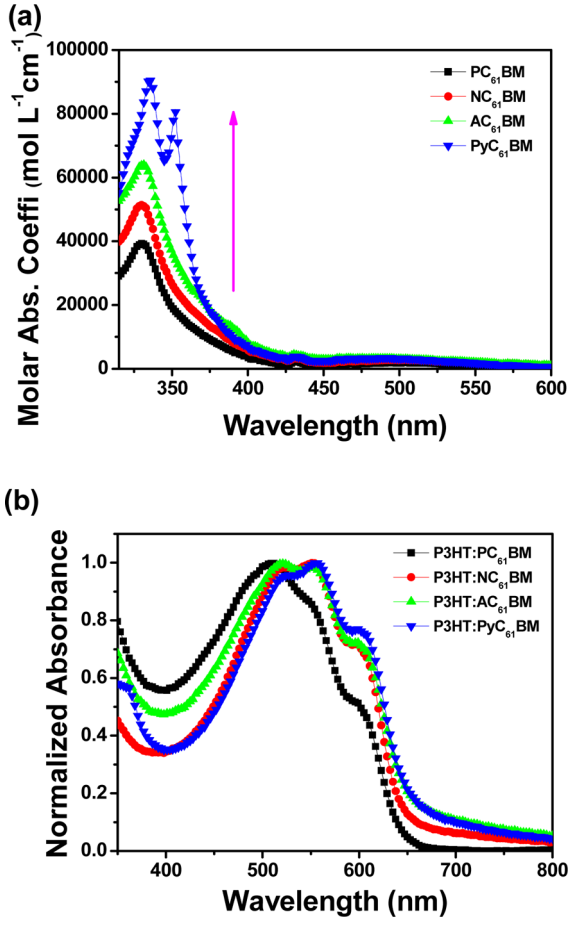

Figure 1. UV−visible absorption spectra of (a) $PC_{61}BM$ and aryl-substituted fullerene derivatives at a 10^{-5} M concentration in 1,2-dichlorobenzene and (b) P3HT:acceptor films.

dx.doi.org/10.1021/am504939c | ACS Appl. Mater. Interfaces 2014, 6, 20776−20785

higher molar absorption coefficients than $PC_{61}BM$, with values of 39 393, 51 452, 64 374, and 91 186 mol L^{-1} cm^{-1} for $PC_{61}BM$, $NC_{61}BM$, $AC_{61}BM$, and $PyC_{61}BM$, respectively. These observations are consistent with what would be expected for a larger π-system. The maximum absorption wavelengths and molar coefficients of $PC_{61}BM$ and aryl-substituted fullerene derivatives are listed in Table 1. The absorption spectra of

Table 1. Optical Properties of $PC_{61}BM$ and Aryl-Substituted Fullerene Derivatives

	10^{-5} mol/L	
acceptor	$\lambda_{max,\ abs}$ (nm)	λ_{max} (M^{-1} cm^{-1})
$PC_{61}BM$	330	39 339
$NC_{61}BM$	330	51 452
$AC_{61}BM$	330	64 374
$PyC_{61}BM$	335, 352	91 186, 81 317

blend films formed from the fullerenes and P3HT (1:0.7, w/w) are shown in Figure 1b. These spectra were similar to each other; the location of the vibronic peak around 600 nm, which is indicative of the ordered structural formation and $\pi-\pi$ stacking of P3HT, was unchanged throughout.[24] The location of the vibronic peaks of the blend films were unchanged, but the position of the absorption maxima of the blend films were slightly bathochromically shifted compared to that of the P3HT:$PC_{61}BM$ blend film. This could be due to slightly different morphology or ordering of P3HT in the blend systems with the fullerene acceptors.[28]

The formation of highly ordered P3HT crystals in the blend films was also indicated by grazing incidence wide-angle X-ray scattering (GIWAXS) measurements[29] shown in Figure 2. The (100), (200), and (300) P3HT diffraction peaks were strongest in the out-of plane direction (q_z), indicating that P3HT had a well-organized structure with stacks oriented along the perpendicular axis of the substrate. From the diffraction pattern, we extract a lamellar spacing of 1.59 nm. Moreover, the (010) diffraction peaks at $q_x \approx 1.65$ $Å^{-1}$ indicated a $\pi-\pi$ stacking distance of 0.38 nm between the P3HT chains in all the samples, consistent with the results in previous reports for P3HT:fullerene blends.[30,31] These results indicate that the crystallinity of P3HT in the blend films was not diminished by the change in bulk of the aryl group in the fullerene derivatives. The most distinct difference among the diffraction patterns among the samples occurs at $q_z \approx 1.4$ $Å^{-1}$, which is due to the presence of an amorphous compound such as $PC_{61}BM$ or aryl-substituted fullerene derivatives. The $q_z \approx 1.4$ $Å^{-1}$ diffraction peak of $NC_{61}BM$ in P3HT blend films is much sharper and more prominent than those of $AC_{61}BM$ and $PyC_{61}BM$ in P3HT blend films. Among these, the diffraction peak of the $AC_{61}BM$ in P3HT blend film showed a particularly broad and diffuse diffraction which may be unfavorable for efficient photovoltaic device operation.[32]

Photoluminescence (PL) spectra were measured of P3HT solutions containing different concentrations of our aryl-substituted fullerene derivatives. Pure P3HT solutions showed a peak emission at 577 nm, which was little changed by addition of fullerenes. The PL intensity of the P3HT solutions was decreased by increasing the fullerene concentration (Figure S4, Supporting Information). To investigate the quenching efficiency of the fullerene acceptors ,we used a Stern–Volmer quenching plot.[33]

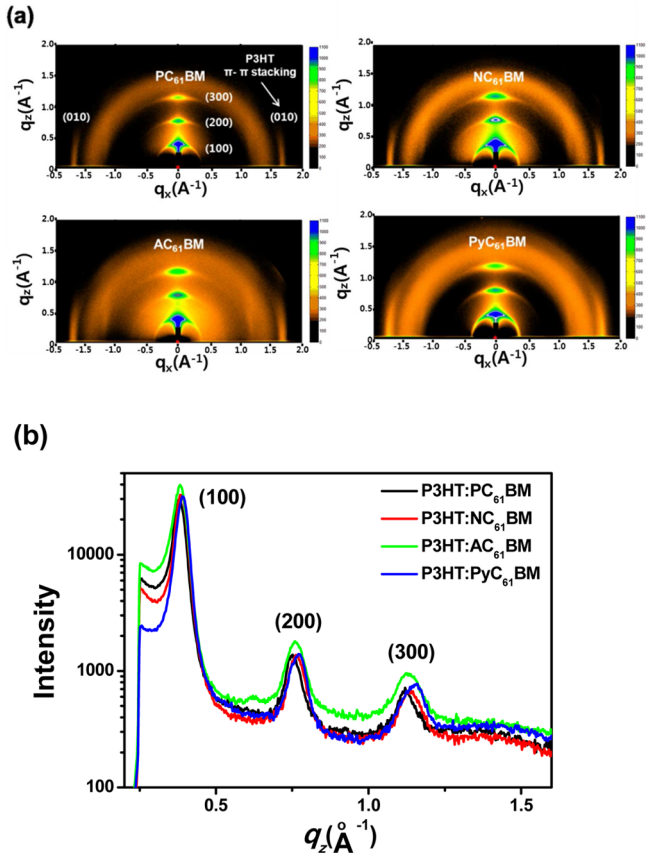

Figure 2. (a) Two-dimensional images and (b) out-of-plane profile for GIWAXS diffraction patterns of P3HT:aryl-substituted fullerene derivative films after annealing at 150 °C for 10 min.

$$I^{o}/I = 1 + K_{sv}[Q]$$

where I^{o} and I are the measured PL intensities in the absence and presence of the quencher, respectively, K_{sv} is the Stern–Volmer quenching constant, and [Q] is the concentration of the quencher. The Stern–Volmer equation provides useful information on intermolecular quenching process. Stern–Volmer quenching plots of P3HT solution with $NC_{61}BM$, $AC_{61}BM$, $PyC_{61}BM$, and $PC_{61}BM$ as the quenchers are shown in Figure 3a. The plots showed a linear regime in the quencher concentration range of $0-10^{-4}$ M. From the plots, we could determine the relative quenching efficiencies of the fullerene acceptors. The calculated K_{sv} values for $PC_{61}BM$, $NC_{61}BM$, $AC_{61}BM$, and $PyC_{61}BM$ were respectively 5.85×10^3, 5.01×10^3, 2.87×10^3, and 4.48×10^3 M^{-1}, respectively. The K_{sv} value can be correlated with a binding affinity between the fluorophore and quencher, thus indicating that $PC_{61}BM$ has the highest binding affinity among the fullerene derivatives toward P3HT, while $NC_{61}BM$ showed a higher K_{sv} value than those of $AC_{61}BM$, and $PyC_{61}BM$.

PL quenching experiment was also conducted for the donor–acceptor blended active films. The pristine P3HT film showed an emission maximum at 646 nm under excitation at 450 nm, and the PL intensity of pristine P3HT film was decreased by blending with the aryl-substituted fullerene derivatives. As shown in Figure 3b, PL emission was quenched by a very high value of 99.3% relative to pristine P3HT in the P3HT:$PC_{61}BM$ blend, whereas it was quenched slightly less in P3HT:$NC_{61}BM$, P3HT:$AC_{61}BM$, and P3HT:$PyC_{61}BM$, with the measured values of 95.8, 89.3, and 93.4%, respectively. The

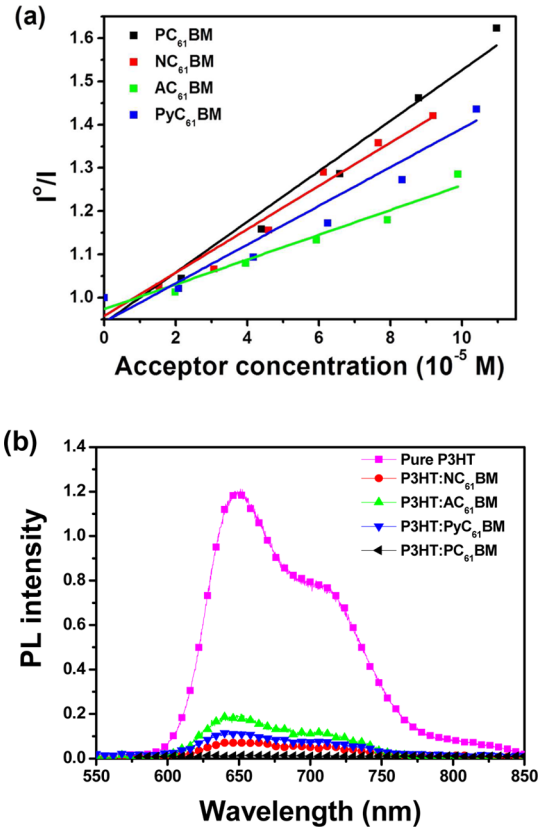

Figure 3. (a) Stern–Volmer plots of P3HT quenching by aryl-substituted fullerene derivatives (10^{-5} M) in solution and (b) PL spectra of pure P3HT and P3HT:aryl-substituted fullerene derivative films.

obtained PL quenching efficiencies are consistent with the K_{sv} values obtained in the donor–acceptor solutions. The electron (i.e., charge) transfer was the most efficient in the P3HT:$PC_{61}BM$ blend system. The electron transfer process is involved in charge separation, and the charge transport properties of active layers of organic photovoltaic devices thus could affect the short-circuit current density of OPVs. The measured K_{sv} and PL quenching efficiencies of the P3HT:fullerene derivative solutions and blends are summarized in Table 2.

Electrochemical Properties. The electrochemical properties of the aryl-substituted fullerene derivatives were investigated by cyclic voltammetry (CV) in 1,2-dichlorobenzene solution, and the measured reduction potential values were compared with those of C_{60} and $PC_{61}BM$. As shown in Figure 4, $PC_{61}BM$, $NC_{61}BM$, $AC_{61}BM$, and $PyC_{61}BM$ exhibited three quasi-reversible reductions. The onset reduction potential values (E^{onset} red) for $PC_{61}BM$, $NC_{61}BM$, $AC_{61}BM$, and $PyC_{61}BM$ were −0.84, −0.86, −0.79, and −0.82 eV, respectively. $NC_{61}BM$ showed a more negative E^{onset} red than $PC_{61}BM$, meaning that it has a higher LUMO energy level than $PC_{61}BM$, while the E^{onset} red of $AC_{61}BM$ and $PyC_{61}BM$ were less negative, indicating lower LUMO levels. Overall, the calculated LUMO energy levels of $PC_{61}BM$, $NC_{61}BM$, $AC_{61}BM$, and $PyC_{61}BM$ were −3.70, −3.68, −3.75, and −3.72 eV, respectively; the value obtained for $PC_{61}BM$ matches that reported in the literature.[34] A relatively high LUMO energy level in the acceptor can result in a high open-circuit voltage value in OPVs devices.[35] The reduction potentials and LUMO energy levels of the aryl-substituted fullerene derivatives are summarized in Table 3.

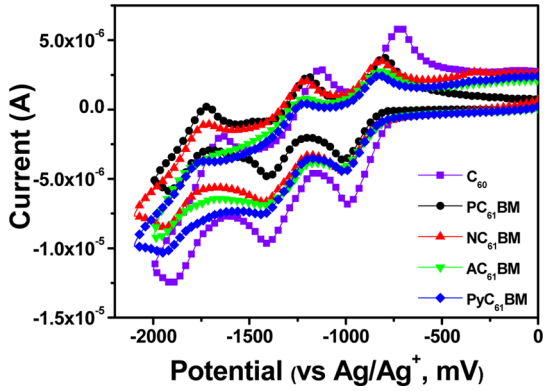

Figure 4. CV data for C_{60}, $PC_{61}BM$, and aryl-substituted fullerene derivatives.

Table 2. Stern–Volmer Quenching Constant (K_{sv}) of P3HT Quenching by Aryl-Substituted Fullerene Derivatives (10^{-5} M) in Solution and Calculated PL Quenching Efficiency for P3HT:Aryl-Substituted Fullerene Derivative Films

	Stern–Volmer eq	PL quenching		
acceptor	K_{sv} (M^{-1})	$I_{acceptor}{}^{a}/I_{P3HT}{}^{b}$	$1-(I_{acceptor}/I_{P3HT})$	quenching efficiency (%)
$PC_{61}BM$	5.85×10^3	0.007	0.993	99.3
$NC_{61}BM$	5.01×10^3	0.042	0.958	95.8
$AC_{61}BM$	2.87×10^3	0.107	0.893	89.3
$PyC_{61}BM$	4.48×10^3	0.066	0.934	93.4

[a]PL intensity in the presence of the acceptor. [b]PL intensity of pure P3HT.

Table 3. Electrochemical Properties of C_{60}, $PC_{61}BM$, and Aryl-Substituted Fullerene Derivatives

acceptor	E^1 red	E^2 red	E^3 red	E^{onset}red	LUMO (eV)[a]
C_{60}	−0.99	−1.41	−1.90	−0.78	−3.77
$PC_{61}BM$	−1.01	−1.40	−1.91	−0.84	−3.70
$NC_{61}BM$	−1.02	−1.42	−1.94	−0.86	−3.68
$AC_{61}BM$	−1.02	−1.42	−1.96	−0.79	−3.75
$PyC_{61}BM$	−1.01	−1.42	−1.95	−0.82	−3.72

[a]LUMO = $-[(E^{onset}\text{ red} - E_{foc}) + 4.8]$ (eV), where E_{foc} is the potential of the ferrocene/ferrocenium ion (Foc/Foc^+) couple used as an external standard.

Charge-Carrier Mobility. Charge-carrier mobilities in the P3HT:$NC_{61}BM$, P3HT:$AC_{61}BM$, and P3HT:$PyC_{61}BM$ films were measured using the space-charge limited current (SCLC) method for both hole-only and electron-only devices. Hole-only ITO/PEDOT:PSS/blend/Au and electron-only ITO/ZnO/blend/LiF/Al devices were fabricated for these measurements; their current density–voltage (J–V) characteristics were measured in the absence of light. The SCLC mobilities were estimated using the Mott–Gurney square law:[36]

$$J = \frac{8}{9}\varepsilon_r\varepsilon_0\mu\frac{V^2}{L^3}$$

dx.doi.org/10.1021/am504939c | ACS Appl. Mater. Interfaces 2014, 6, 20776–20785

where J is the current density, ε_r is the dielectric constant of the fullerene derivative, ε_o is the permittivity of the vacuum, μ is the hole or electron mobility, L is the film thickness, and $V = V_{appl} - V_{bi}$, where V_{appl} is the applied potential and V_{bi} is the built-in voltage that results from the difference in the work functions of the anode and the cathode. Figure 5a shows the $J-V$ curves of

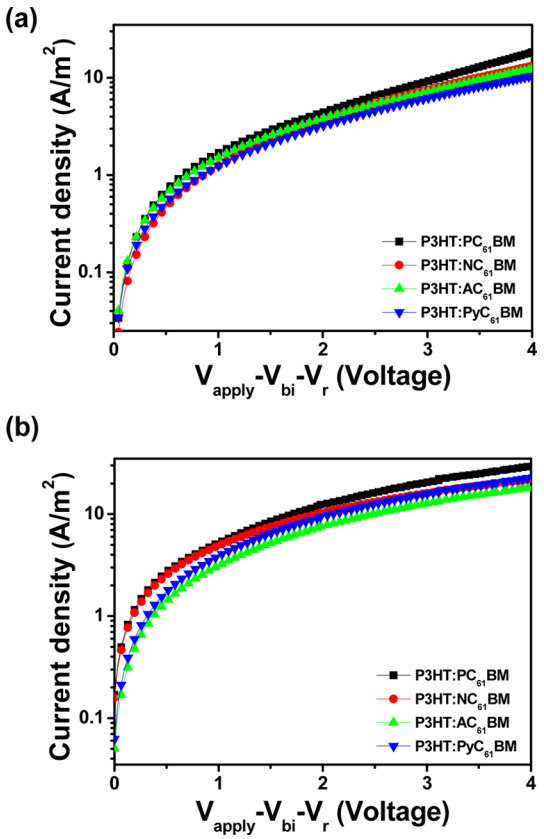

Figure 5. Measured space-charge limited current $J-V$ characteristics of P3HT:PC_{61}BM and P3HT:aryl-substituted fullerene derivative devices for (a) hole- and (b) electron-only devices.

the P3HT:PC_{61}BM, P3HT:NC_{61}BM, P3HT:AC_{61}BM, and P3HT:PyC_{61}BM films for hole-only devices, which indicate very similar hole mobility values of 3.37×10^{-4}, 3.05×10^{-4}, 3.11×10^{-4}, and 3.08×10^{-4} cm^2 V^{-1} s^{-1}, respectively. Meanwhile, Figure 5b shows the corresponding data for electron-only devices, with P3HT:PC_{61}BM, P3HT:NC_{61}BM, P3HT:AC_{61}BM, and P3HT:PyC_{61}BM films exhibiting electron-mobility values of 2.39×10^{-4}, 2.27×10^{-4}, 1.75×10^{-4}, and 2.13×10^{-4} cm^2 V^{-1} s^{-1}, respectively; the measured value for P3HT:PC_{61}BM is close to that reported in the literature.[24,37] Overall, electron mobility of the P3HT:NC_{61}BM film was similar to that of the P3HT:PC_{61}BM film, whereas the P3HT:AC_{61}BM and P3HT:PyC_{61}BM films exhibited lower electron mobilities, with P3HT:AC_{61}BM showing the lowest. It is known that well-balanced charge-carrier transport is an important factor for increasing the fill factor (FF) of BHJ solar cells;[38,39] therefore, we further compared the hole to electron mobility ratios (μ_h/μ_e), which we found to be different for different films. The P3HT:NC_{61}BM film exhibited a markedly more balanced μ_h/μ_e value than all other films; indeed, it has a slightly better-balanced μ_h/μ_e value than the P3HT:PC_{61}BM film.[41] Meanwhile, P3HT:AC_{61}BM showed the least balanced μ_h/μ_e due to its lower electron mobility, while P3HT:PyC_{61}BM showed similar characteristics to P3HT:PC_{61}BM. The calculated parameters by the SCLC method are summarized in Table 4.

Table 4. Calculated Hole and Electron Mobility Values of P3HT:PC_{61}BM and P3HT:Aryl-Substituted Fullerene Derivative Films Using the SCLC Method

P3HT:acceptor	M_H (Cm^2 V^{-1} S^{-1})	M_E (Cm^2 V^{-1} S^{-1})	M_H/M_E
P3HT:Pc_{61}Bm	3.37×10^{-4}	2.39×10^{-4}	1.41
P3HT:Nc_{61}Bm	3.05×10^{-4}	2.27×10^{-4}	1.34
P3HT:Ac_{61}Bm	3.11×10^{-4}	1.75×10^{-4}	1.78
P3HT:Pyc_{61}Bm	3.08×10^{-4}	2.13×10^{-4}	1.45

Photovoltaic Properties. Photovoltaic devices were fabricated using P3HT as the electron donor and the aryl-substituted fullerene derivatives as the electron acceptors. To determine the optimum device conditions, we varied the donor to acceptor blend ratios (1:0.5, 1:0.7, and 1:1) for each of the different active layer, and the spin-coated active layers were annealed at 150 °C for 10 min (Figure S5, Supporting Information). A blend ratio of 1:0.7 (w/w) P3HT:fullerene derivative and a film thickness of 100 nm were found to provide optimal performance. Figure 6a shows the $J-V$ curves of the OPVs using P3HT:aryl-substituted fullerene derivatives (1:0.7, w/w) with annealing at 150 °C for 10 min. The photovoltaic characteristics of the fabricated devices at the optimal blend ratio, including the open-circuit voltage (V_{oc}), short-circuit current density (J_{sc}), and fill factor (FF), are summarized in Table 5, using the P3HT:PC_{61}BM values as a reference.

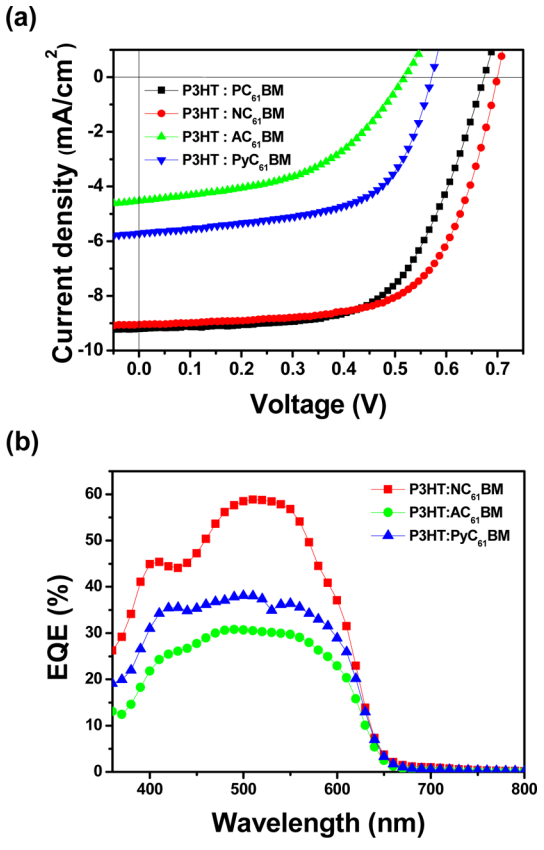

Figure 6. (a) $J-V$ curves and (b) EQE curves of P3HT:aryl-substituted fullerene derivative OPVs annealed at 150 °C for 10 min.

dx.doi.org/10.1021/am504939c | ACS Appl. Mater. Interfaces 2014, 6, 20776−20785

Detailed photovoltaic performances for devices with different blend ratios are listed in Figure S5 (Supporting Information).

Table 5. Photovoltaic Performance of OPVs Based on a Blend of P3HT and Aryl-Substituted Fullerene Derivatives Annealed at 150 °C for 10 min and Measured under AM 1.5G Illumination of 100 mW/cm^2

P3HT:acceptor	ratio	V_{oc} (V)	J_{sc} (mA/cm^2)	FF	PCE (%)
P3HT:NC_{61}BM	1:0.5	0.70	8.86	0.55	3.40
	1:0.7	0.70	9.06	0.64	4.09
	1:1	0.70	8.21	0.64	3.66
P3HT:AC_{61}BM	1:0.5	0.50	3.66	0.51	0.95
	1:0.7	0.52	4.53	0.49	1.14
	1:1	0.54	3.80	0.40	0.81
P3HT:PyC_{61}BM	1:0.5	0.57	5.29	0.58	1.72
	1:0.7	0.57	5.71	0.60	1.95
	1:1	0.56	4.14	0.55	1.29
P3HT:PC_{61}BM	1:0.7	0.67	9.21	0.61	3.80

The highest PCE values observed for P3HT:PC_{61}BM, P3HT:NC_{61}BM, P3HT:AC_{61}BM, and P3HT:PyC_{61}BM were 3.80, 4.09, 1.14, and 1.95%, respectively. The V_{oc} values for the P3HT:PC_{61}BM, P3HT:NC_{61}BM, P3HT:AC_{61}BM, and P3HT:PyC_{61}BM devices were 0.67, 0.70, 0.52, and 0.57 V, respectively. The P3HT:NC_{61}BM device showed a higher V_{oc} value than that of the P3HT:PC_{61}BM device, while the values for P3HT:AC_{61}BM and P3HT:PyC_{61}BM were lower than expected, seeing as how V_{oc} values are directly related to the energy gap between the LUMO level of the electron acceptor and the highest occupied molecular orbital (HOMO) level of the electron donor. The 30 mV increase in the V_{oc} value of the P3HT:NC_{61}BM device when compared to the P3HT:PC_{61}BM device is therefore consistent with the LUMO level of NC_{61}BM being 20 mV higher than that of PC_{61}BM according to electrochemical measurements. Similarly, because AC_{61}BM and PyC_{61}BM had lower LUMO levels than that of PC_{61}BM, their devices had lower V_{oc} values; unsurprisingly, the P3HT:AC_{61}BM device had both the lowest LUMO energy level (−3.75 eV) and the lowest V_{oc} value (0.52 V) among all the four devices.

The measured J_{sc} values for the P3HT:PC_{61}BM, P3HT:NC_{61}BM, P3HT:AC_{61}BM, and P3HT:PyC_{61}BM devices were 9.21, 9.06, 4.53, and 5.71 mA/cm^2, respectively, giving the P3HT:PC_{61}BM device the highest value; while the P3HT:NC_{61}BM device did exhibit similar value, and the J_{sc} value of the P3HT:AC_{61}BM, and P3HT:PyC_{61}BM devices showed notably lower value than the P3HT:NC_{61}BM device. The relatively high J_{sc} value seen for the P3HT:NC_{61}BM device is likely related to its more efficient PL quenching and relatively high electron mobility.

The P3HT:NC_{61}BM device showed a higher FF value (0.64) than either the P3HT:AC_{61}BM (0.49) or P3HT:PyC_{61}BM devices (0.60); indeed, it was even higher than that of the P3HT:PC_{61}BM device (0.61). This result could be explained by the charge balance values measured by the SCLC method. The P3HT:NC_{61}BM blend with the high device FF exhibited a relatively more well-balanced μ_h/μ_e value by the SCLC method than that of the other blends, while the P3HT:AC_{61}BM device that had the lowest FF value also had the poorest balance of μ_h/μ_e.

Figure 6b shows the external quantum efficiency (EQE) curves of the best devices. Overall, EQE values in the range 400−600 nm are mainly due to the absorption by P3HT. The maximum EQEs of the P3HT:NC_{61}BM, P3HT:AC_{61}BM, and P3HT:PyC_{61}BM devices are 58.9% (at 510 nm), 38.1% (at 500 nm), and 30.8% (at 490 nm), respectively. The EQE value of the P3HT:NC_{61}BM device is higher than that for P3HT:AC_{61}BM and P3HT:PyC_{61}BM, an observation that is consistent with the J_{sc} values obtained in the fabricated devices.

Morphology. Atomic force microscopy (AFM) was used for understanding the effect of the morphology of the photoactive layers of the fabricated films on the photovoltaic performance of P3HT-based OPVs;[40] the resulting images are shown in Figure 7. The active layer films were annealed at 150 °C for 10 min, which we found to be the optimum device fabrication conditions. It can clearly be seen that the size of the P3HT domains and the extent of phase separation between the donor and the acceptor were highly uniform in all the films.

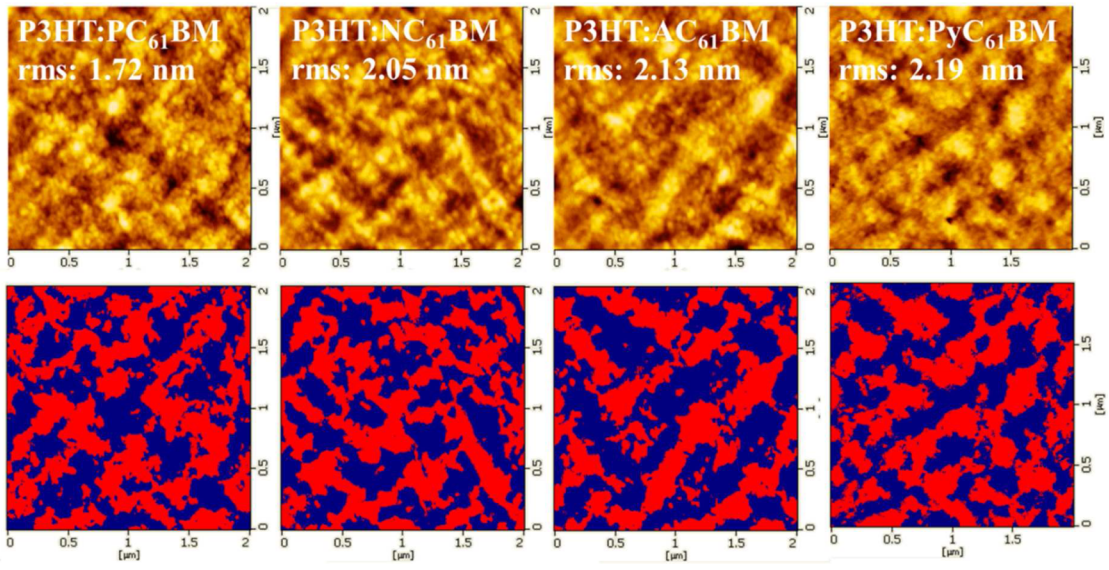

Figure 7. AFM images of (a) P3HT:PC_{61}BM, (b) P3HT:NC_{61}BM, (c) P3HT:AC_{61}BM, and (d) P3HT:PyC_{61}BM films.

The brighter islands represent aggregated P3HT, while the darker valleys represent the fullerene derivatives. The surface root-mean-square (rms) roughness values for the P3HT:$PC_{61}BM$, P3HT:$NC_{61}BM$, P3HT:$AC_{61}BM$, and P3HT:$PyC_{61}BM$ films were 1.72, 2.05, 2.04, and 2.13 nm, respectively. In general, a rough surface in P3HT-based blend films indicates P3HT self-organization, an effect which enhances the formation of ordered structures.[41] The observed mean diameters of P3HT domains in P3HT:$PC_{61}BM$, P3HT:$NC_{61}BM$, P3HT:$AC_{61}BM$, and P3HT:$PyC_{61}BM$ blend films were 144, 138, 193, and 157 nm, respectively. The P3HT domains in P3HT:$PC_{61}BM$, P3HT:$NC_{61}BM$ blend films were better interconnected than those in P3HT:$AC_{61}BM$ and P3HT:$PyC_{61}BM$ films. The $AC_{61}BM$ clusters in P3HT-blend films showed larger cluster size than those of $PC_{61}BM$, $NC_{61}BM$, and $PyC_{61}BM$, and this would increase the mean distance between polymer−fullerene interfaces and decrease the total interfacial area. This result is consistent with the low current output of the device fabricated using $AC_{61}BM$.[42−44]

CONCLUSIONS

We have successfully synthesized new aryl-substituted fullerene derivatives, $NC_{61}BM$, $AC_{61}BM$, and $PyC_{61}BM$, whose absorption spectra were similar to each other and to that of $PC_{61}BM$. The LUMO energy level of $NC_{61}BM$ was somewhat higher than that of $PC_{61}BM$, while those of the others were slightly lower. $NC_{61}BM$, $AC_{61}BM$, and $PyC_{61}BM$ were then used as electron acceptors in the fabrication of P3HT-based BHJ solar cells with the device structure of ITO/PEDOT:PSS/P3HT:acceptor/LiF/Al. The highest PCE values observed for $NC_{61}BM$, $AC_{61}BM$, and $PyC_{61}BM$ were 4.09, 1.14, and 1.95%, respectively, compared to a value of 3.80% for $PC_{61}BM$. The higher PCE value of the $NC_{61}BM$-based device likely resulted from its higher V_{oc} and FF values due to its higher LUMO energy level and more balanced charge carrier mobility, respectively, when compared to $PC_{61}BM$. Therefore, among the three aryl-substituted fullerene derivatives, $NC_{61}BM$ appears to be the most promising acceptor candidate for producing highly efficient OPVs.

EXPERIMENTAL SECTION

Materials. Naphthalene, anthracene, pyrene, methyl 5-chloro-5-oxopentanoate, aluminum trichloride, *p*-toluene-sulfonylhydrazide, hydrogen chloride, sodium methoxide, pyridine, and 1,2-dichlorobenzene were purchased from Aldrich. Fullerene (C_{60}) was purchased from Nano-C. All chemicals were used without further purification.

Measurements. ^1H and ^{13}C NMR spectra were recorded using a Varian 300 spectrometer. FAB-MS spectra were measured using a ZMS-DX303 mass spectrometer (JEOL Ltd.), while absorption spectra were measured using a Model S-300 Scinco UV−vis spectrophotometer. Photoluminescence (PL) spectra were recorded using a Shimadzu F-7000 FL Spectrophotometer. TGA was performed on a TGA Q500 V6.7 Build 203 (TA Instruments), using a 2910 MDSC V4.4E (TA Instruments) analyzer under a N_2 atmosphere with a heating and cooling rate of 10 °C/min. High-performance liquid chromatography (HPLC) spectra were recorded using a WatersTM 600 Controller with WatersTM 486 tunable absorbance detector. AFM was completed using SPM L-Trace II operating in the tapping mode in air after annealing at 150 °C for 10 min. CV (CH Instruments 600D) was performed with a 0.10 M solution of tetrabutylammonium tetrafluoroborate in 1,2-dichlorobenzene, with the analyte present in a concentration of 10^{-3} M and employing a scan rate of 100 mV/s at room temperature under argon atmosphere. A Pt electrode was used as the working electrode, while a Pt wire and a Ag/Ag^+ electrode were used as the counter electrode and reference electrode, respectively. SCLC hole and electron mobility measurements were completed using ITO/PEDOT:PSS/blend/Au and ITO/ZnO/blend/LiF/Al devices, respectively. GIWAXS measured at the 4C2 beamline in the Pohang Accelerator Laboratory (PAL, South Korea). 2D GIWAXS patterns were recorded using CCD detector positioned at the end of a vacuum guide tube in which the X-ray pass through the thin films under vacuum, where operation conditions were set to a X-ray wavelength of 1.3807 Å and a sample-to-detector distance (SDD) of 122.83. The incidence angle was carefully chosen to allow for complete X-ray penetration of the film. The scattering spectra were collected as a 2D image map oriented along the plane of the substrate (q_x) and the plane perpendicular to the substrate (q_z).

Fabrication of Photovoltaic Devices. Composite solutions of P3HT and aryl-substituted fullerene derivatives were prepared using 1,2-dichlorobenzene as a solvent. The concentration was kept within the range of 1.0−2.0 wt %. Polymer photovoltaic devices employing an ITO/PEDOT:PSS/P3HT:acceptor/LiF/Al sandwich structure were then fabricated. The ITO-coated glass substrates were cleaned by sonication in a detergent solution followed by sonication successively in distilled water, acetone, and 2-propanol. A 40 nm thick layer of PEDOT:PSS (Clevious P VP AI4083) was then spin-coated onto the cleaned ITO substrate after exposing the ITO surface to ozone for 10 min. This PEDOT:PSS layer was baked on a hot plate at 150 °C for 15 min, after which the composite solution was filtered using a 0.45-μm syringe filter and spin-coated on the PEDOT:PSS layer at 900 rpm up to a thickness of 100 nm. Finally, a top electrode consisting of a 0.5 nm thick layer of LiF and a 120 nm thick layer of Al was deposited on the polymer active layer in a thermal evaporator under a vacuum of 3×10^{-6} Torr.

The $J-V$ characteristics of all photovoltaic cells were analyzed under simulated solar light (intensity: 100 mW/cm^2; AM 1.5G) provided by an Oriel 300 W solar simulator. Electric data were recorded using a Keithley 2400 source-measure unit, and all characterizations were carried out in an ambient environment. The intensity of the simulated sunlight used was calibrated using a standard Si photodiode detector (BS520, Bunkoh-keiki) that had been calibrated at National Renewable Energy Laboratory (NREL). EQE values were measured as a function of wavelength from 360 to 800 nm using a device (PV Measurements, Inc.) equipped with a halogen lamp light source, while calibration was performed using the Si reference photodiode. The measurement was carried out after masking all but the active cell area of the fabricated device. All characterization steps were carried out under ambient laboratory atmosphere. The active area of the solar cells was 9 mm^2. The thickness of the thin film was measured using a KLA Tencor Alpha-step IQ surface profilometer with an accuracy of ±1 nm.

Synthesis of Aryl-Substituted Fullerene Derivatives. *Synthesis of Methyl 5-(Naphthalen-2-yl)-5-oxopentanoate (**1**).* To a solution of naphthalene (3.0 g, 23.41 mmol) in dichloromethane (150 mL) was added methyl 5-chloro-5-oxopentanoate (5.77 g, 35.06 mmol). Aluminum trichloride (6.24 g, 46.8 mmol) was added to the solution, and the resulting mixture was first stirred at 0 °C for 30 min and then warmed to room temperature. After stirring overnight, the reaction was quenched by the dropwise addition of an aqueous solution of 2 M HCl, after which the mixture was partitioned between dichloromethane and brine. The organic layer was dried with anhydrous $MgSO_4$ and then concentrated under reduced pressure. The crude product was purified by column chromatography using hexane/ethyl acetate as the eluent to give **1** (2.75 g, 45.8%). ^1H NMR (300 MHz, $CDCl_3$) δ (ppm): 8.48 (s, 1H), 8.04 (d, 1H), 7.97 (d, 1H), 7.87 (t, 2H), 7.56 (m, 2H), 3.69 (s, 3H), 3.20 (t, 2H), 2.49 (t, 2H), 2.13 (m, 2H). ^{13}C NMR (75 MHz, $CDCl_3$) δ (ppm): 199.447, 173.915, 135.763, 134.338, 132.717, 129.873, 129.758, 128.629, 127.961, 126.963, 123.986, 51.771, 37.702, 33.368, 19.696.

*Synthesis of Methyl 5-(Anthracen-9-yl)-5-oxopentanoate (**2**).* Compound **2** was prepared from anthracene by the same procedure used to make **1** (2.43 g, 47.1%). ^1H NMR (300 MHz, $CDCl_3$) δ (ppm): 9.34 (s, 1H), 8.45 (s, 1H), 8.17 (d, 1H), 7.98 (m, 3H), 7.51 (m, 3H), 3.69 (s, 3H), 3.21 (t, 2H), 2.52 (t, 2H), 2.19 (m, 2H). ^{13}C NMR (75 MHz, $CDCl_3$) δ (ppm): 203.440, 173.915, 135.316, 133.801, 133.160, 132.141, 131.767, 129.342, 128.724, 128.007,

127.891, 127.165, 126.381, 126.231, 125.675, 123.696, 51.836, 40.776, 33.449, 20.117.

*Synthesis of Methyl 5-oxo-5-(Pyren-1-yl) pentanoate (**3**).* Compound **3** was prepared from pyrene by the same procedure used to make **1** (2.2 g, 44.5%). ^{1}H NMR (300 MHz, $CDCl_3$) δ (ppm): 8.93 (d, 1H), 8.34 (d, 1H), 8.23 (m, 5H), 8.09 (d, 2H), 3.69 (s, 3H), 3.29 (t, 2H), 2.53 (t, 2H), 2.21 (m, 2H). ^{13}C NMR (75 MHz, $CDCl_3$) δ (ppm): 203.810, 173.916, 133.837, 132.129, 131.147, 130.597, 129.705, 129.565, 129.466, 127.137, 126.477, 126.390, 126.337, 126.116, 125.009, 124.940, 124.333, 124.113, 51.814, 41.355, 33.483, 20.232.

*Synthesis of (E)-Methyl 5-(Naphthalen-2-yl)-5-(2-tosylhydrazono) Pentanoate (**4**).* Compound **1** (2.5 g, 9.75 mmol) and *p*-toluenesulfonylhydrazide (2.72 g, 14.6 mmol) were dissolved in methanol (250 mL). A catalytic amount of HCl was added to the mixture, which was then refluxed for 12 h. The resulting mixture was partitioned between dichloromethane and brine, and the organic layer was dried with anhydrous $MgSO_4$. The crude product was purified by column chromatography using hexane/ethyl acetate as the eluent. The resulting solid was recrystallized from dichloromethane and hexane, and the resulting white solid was dried in vacuo to give **4** as a white powder (2.76 g, 66.7%). ^{1}H NMR (300 MHz, $CDCl_3$) δ (ppm): 9.37 (s, 1H), 7.95 (m, 4H), 7.82 (t, 3H), 7.48 (m, 2H), 7.32 (t, 2H), 3.83 (s, 3H), 2.74 (t, 2H), 2.39 (m, 5H), 1.78 (m, 2H); ^{13}C NMR (75 MHz, $CDCl_3$) δ (ppm).: 175.010, 153.597, 143.993, 136.271, 134.018, 133.843, 133.169, 129.731, 128.713, 128.381, 128.185, 127.833, 127.075, 126.602, 126.105, 123.888, 52.612, 32.341, 25.937, 21.806, 21.306.

*Synthesis of (E)-Methyl 5-(Anthracen-9-yl)-5-(2-tosylhydrazono) Pentanoate (**5**).* Compound **5** was prepared from **2** by the same procedure used to make **4** (1.63 g, 52.6%). ^{1}H NMR (300 MHz, $CDCl_3$) δ (ppm): 8.50 (s, 1H), 8.09(d, 1H), 8.03 (d, 1H), 7.68 (d, 2H), 7.58 (d, 2H), 7.48 (m, 3H), 7.34 (d, 2H), 7.21 (s, 1H), 7.14 (d, 1H), 3.62 (s, 3H), 2.68 (t, 2H), 2.54 (s, 3H), 2.33 (t, 2H), 1.92 (m, 2H). ^{13}C NMR (75 MHz, $CDCl_3$) δ (ppm): 173.715, 157.223, 144.286, 135.630, 132.452, 131.333, 130.890, 129.773, 129.015, 128.217, 127.321, 127.254, 126.905, 126.850, 126.453, 126.173, 125.711, 124.983, 124.645, 124.439, 123.024, 51.773, 38.425, 33.445, 21.938, 21.536.

*Synthesis of (E)-Methyl 5-(Pyren-1-yl)-5-(2-tosylhydrazono) Pentanoate (**6**).* Compound **6** was prepared from **3** by the same procedure used to make **4** (1.96 g, 64.9%). ^{1}H NMR (300 MHz, $CDCl_3$) δ (ppm): 9.23 (s, 1H), 8.35 (m, 8H), 7.81 (m, 2H), 7.57 (d, 1H), 7.49 (d, 2H), 3.59 (s, 3H), 2.69 (t, 2H), 2.50 (s, 3H), 2.39 (t, 2H), 2.13 (m, 2H). ^{13}C NMR (75 MHz, $CDCl_3$) δ (ppm): 173.738, 156.944, 144.233, 144.207, 135.617, 132.380, 132.301, 131.628, 130.985, 130.739, 129.916, 128.594, 128.320, 128.129, 128.021, 126.508, 126.330, 126.264, 125.090, 124.802, 122.552, 51.780, 37.961, 33.425, 21.939, 21.497.

Synthesis of $NC_{61}BM$. Compound **4** (0.5 g, 1.18 mmol) and sodium methoxide (0.13 g, 2.41 mmol) were dissolved in dry pyridine (20 mL) under nitrogen. The mixture was stirred at room temperature for 30 min. To the mixture, a solution of C_{60} (0.68 g, 0.94 mmol) in 1,2-dichlorobenzene (250 mL) was added, and the mixture was stirred at 80 °C under nitrogen for 48 h. The mixture was then heated to 180 °C and stirred overnight. After the mixture cooled to room temperature, the solvent was removed by distillation, and the residue was purified by column chromatography using toluene as the eluent. The crude product was purified by several reprecipitations in methanol followed by extraction with hexane and methanol in a Soxhlet extractor to give $NC_{61}BM$ as a dark brown solid (305 mg, 26.9%). ^{1}H NMR (300 MHz, $CDCl_3$) δ (ppm): 8.36 (s, 1H), 8.04 (m, 2H), 7.98 (m, 2H), 7.59 (m, 2H), 3.65 (s, 3H), 2.97 (t, 2H), 2.52 (t, 2H), 2.23 (m, 2H). ^{13}C NMR (75 MHz, $CDCl_3$) δ (ppm): 173.655, 148.013, 146.113, 145.419, 145.339, 145.267, 145.024, 144.906, 144.743, 144.690, 144.246, 143.981, 143.287, 143.176, 142.482, 142.357, 141.246, 141.007, 138.324, 134.269, 133.245, 133.127, 131.940, 129.352, 128.723, 128.469, 128.108, 126.894, 126.754, 52.084, 51.886, 34.124, 31.146, 22.702. FAB-MS (M+1, $C_{76}H_{16}O_2$): Calcd, 960.12. Found, 960. Elemental analysis for $C_{76}H_{16}O_2$: Calcd, C, 94.99; H, 1.68; O, 3.33. Found, C, 95.54; H, 1.91; O, 1.99 (purity, 98.43% by HPLC).

Synthesis of $AC_{61}BM$. $AC_{61}BM$ was prepared from **5** by the same procedure used to make $NC_{61}BM$ (110 mg, 10.8%). ^{1}H NMR (300 MHz, $CDCl_3$) δ (ppm): 9.41 (s, 1H), 8.66 (s, 1H), 8.21(d, 1H), 8.13 (m, 2H), 7.63 (m, 2H), 7.55 (m, 2H), 3.61 (s, 3H), 3.38 (t, 2H), 3.18 (t, 2H), 2.52 (m, 2H). ^{13}C NMR (75 MHz, $CDCl_3$) δ (ppm): 173.632, 148.916, 148.025, 146.120, 145.430, 145.274, 145.032, 144.914, 144.747, 144.698, 144.250, 143.985, 143.294, 143.188, 142.494, 142.365, 141.253, 141.014, 138.332, 134.280, 133.260, 133.142, 131.940, 129.349, 128.723, 128.472, 128.116, 126.898, 126.758, 52.095, 51.871, 34.128, 33.889, 22.735. FAB-MS (M+1, $C_{80}H_{18}O_2$): Calcd, 1010.13. Found, 1011. Elemental analysis for $C_{80}H_{18}O_2$: Calcd, C, 95.04; H, 1.79; O, 3.17. Found, C, 94.33; H, 2.20; O, 2.31 (purity, 97.58% by HPLC).

Synthesis of $PyC_{61}BM$. $PyC_{61}BM$ was prepared from **6** by the same procedure used to make $NC_{61}BM$ (225 mg, 21.7%). ^{1}H NMR (300 MHz, $CDCl_3$) δ (ppm): 9.21 (d, 1H), 8.56 (d, 1H), 8.25 (m, 5H), 8.05 (m, 2H), 3.59 (s, 3H), 2.38 (t, 2H), 3.17 (t, 2H), 2.42 (m, 2H). ^{13}C NMR (75 MHz, $CDCl_3$) δ (ppm): 173.579, 149.076, 147.558, 146.249, 145.434, 145.309, 144.941, 144.868, 144.041, 143.165, 143.165, 142.387, 142.300, 137.156, 132.596, 131.720, 131.526, 130.912, 130.206, 129.705, 129.034, 128.302, 127.771, 126.557, 126.158, 126.067, 124.296, 123.738, 51.822, 50.578, 34.166, 33.123, 23.971. FAB-MS (M+1, $C_{82}H_{18}O_2$): Calcd, 1035.02. Found, 1035. Elemental analysis for $C_{82}H_{18}O_2$: Calcd, C, 95.16; H, 1.75; O, 3.09. Found, C, 95.61; H, 1.86; O, 1.76 (purity, 98.64% by HPLC).

■ ASSOCIATED CONTENT

Ⓢ Supporting Information

^{1}H NMR spectra and FAB-mass spectra of aryl-substituted fullerene derivatives, TGA curves, and OPV parameter data. This material is available free of charge via the Internet at http://pubs.acs.org.

■ AUTHOR INFORMATION

Corresponding Author

*Tel.: +82 51 510 2232. Fax: +82 51 516 7421. E-mail: dohoonhwang@pusan.ac.kr.

Notes

The authors declare no competing financial interest.

■ ACKNOWLEDGMENTS

This work was supported by the Center for Advanced Soft-Electronics funded by the Ministry of Science, ICT, and Future Planning as Global Frontier Project (CASE-2014M3A6A5060936), and a National Research Foundation (NRF) grant funded by the Korean government (NRF-2014R1A2A2A01007318 and No. 2011-0030668 through GCRC SOP).

■ REFERENCES

(1) Thompson, B. C.; Fréchet, J. M. J. Polymer-Fullerene Composite Solar Cells. *Angew. Chem., Int. Ed.* **2008**, *47*, 58−77.

(2) Cheng, Y.-J.; Yang, S.-H.; Hsu, C.-S. Synthesis of Conjugated Polymer for Organic Solar Cells Applications. *Chem. Rev.* **2009**, *109*, 5868−5923.

(3) Brabec, C. J.; Sariciftci, N. S.; Hummelen, J. C. Plastic Solar Cells. *Adv. Funct. Mater.* **2011**, *11*, 15−26.

(4) Nielsen, T. D.; Cruickshank, C.; Foged, S.; Thorsen, J.; Krebs, F. C. Business, Market, and Intellectual Property Analysis of Polymer Solar Cells. *Sol. Energy Mater. Sol. Cells* **2010**, *94*, 1553−1571.

(5) Sun, Y.; Welch, G. C.; Leong, W. L.; Takacs, C. J.; Bazan, G. C. Solution-Processed Small-Molecule Solar Cells with 6.7% Efficiency. *Nat. Mater.* **2012**, *11*, 44−48.

(6) Hummelen, J. C.; Knight, B. W.; Lepeq, F.; Wudl, F. Preparation and Characterization of Fulleroid and Methanofullerene Derivatives. *J. Org. Chem.* **1995**, *60*, 532−538.
(7) Janssen, R. A. J.; Hummelen, J. C.; Lee, K.; Pakbaz, K.; Sariciftci, N. S.; Heeger, A. J.; Wudl, F. Photoinduced Electron Transfer from π-conjugated Polymers onto Buckminsterfullerene, Fulleroids, and Methanofullerenes. *J. Chem. Phys.* **1995**, *103*, 788−793.
(8) Yu, G.; Gao, J.; Hummelen, J. C.; Wudl, F.; Heeger, A. J. Polymer Photovoltaic Cells: Enhanced Efficiencies via a Network of Internal Donor-Acceptor Heterojunctions. *Science* **1995**, *270*, 1789−1791.
(9) Granström, M.; Petrisch, K.; Arias, A. C.; Lux, A.; Andersson, M. R.; Friend, R. H. Laminated Fabrication of Polymeric Photovoltaic Diodes. *Nature* **1998**, *395*, 257−260.
(10) Dennler, G.; Scharber, M. C.; Brabec, C. J. Polymer-Fullerene Bulk-Heterojunction Solar Cells. *Adv. Mater.* **2009**, *21*, 1323−1338.
(11) Li, Y.; Zou, Y. Conjugated Polymer Photovoltaic Materials with Broad Absorption Band and High Charge Carrier Mobility. *Adv. Mater.* **2008**, *20*, 2952−2958.
(12) Chen, J.; Cao, Y. Development of Novel Conjugated Donor Polymers for High-Efficiency Bulk-Heterojunction Photovoltaic Devices. *Acc. Chem. Res.* **2009**, *42*, 1709−1718.
(13) Zhang, Y.; Yip, H.-L.; Acton, O.; Hau, S. K.; Huang, F.; Jen, A. K.-Y. A Simple and Effective Way of Achieving Highly Efficient and Thermally Stable Bulk-Heterojunction Polymer Solar Cells Using Amorphous Fullerene Derivatives as Electron Acceptor. *Chem. Mater.* **2009**, *21*, 2598−2600.
(14) Yang, C.; Kim, J. Y.; Cho, S.; Lee, J. K.; Heeger, A. J.; Wudl, F. Functionalized Methanofullerenes Used as n-Type Materials in Bulk-Heterojunction Polymer Solar Cells and in Field-Effect Transistors. *J. Am. Chem. Soc.* **2008**, *130*, 6444−6450.
(15) Troshin, P. A.; Hoppe, H.; Renz, J.; Egginger, M.; Mayorova, J. Y.; Goryachev, A. E.; Peregudov, A. S.; Lyubovskaya, R. N.; Gobsch, G.; Sariciftci, N. S.; Razumov, V. F. Material Solubility-Photovoltaic Performance Relationship in the Design of Novel Fullerene Derivatives for Bulk-Heterojunction Solar Cells. *Adv. Funct. Mater.* **2009**, *19*, 779−788.
(16) Zhao, G.; He, Y.; Xu, Z.; Hou, J.; Zhang, M.; Min, J.; Chen, H.-Y.; Ye, M.; Hong, Z.; Yang, Y.; Li, Y. Effect of Carbon Chain Length in the Substituents of PCBM-like Molecules on Their Photovoltaic Properties. *Adv. Funct. Mater.* **2010**, *20*, 1480−1487.
(17) Backer, S. A.; Sivula, K.; Kavulak, D. F.; Fréchet, J. M. J. High Efficiency Organic Photovoltaics Incorporating a New Family of Soluble Fullerene Derivatives. *Chem. Mater.* **2007**, *19*, 2927−2929.
(18) Zhao, G.; He, Y.; Li, Y. 6.5% Efficiency of Polymer Solar Cells Based on Poly(3-hexylthiophene) and Indene-C_{60} Bisadduct by Device Optimization. *Adv. Mater.* **2010**, *22*, 4355−4358.
(19) Mikroyannidis, J. A.; Kabanakis, A. N.; Sharma, S. S.; Sharma, G. D. A Simple and Effective Modification of PCBM for Use as an Electron Acceptor in Efficient Bulk Heterojunction Solar Cells. *Adv. Funct. Mater.* **2011**, *21*, 746−755.
(20) Saravanan, C.; Liu, C.-L.; Chang, Y.-M.; Lu, J.-D.; Hsieh, Y.-J.; Rwei, S.-P.; Wang, L. [60]Fulleropyrrolidines Bearing π-Conjugated Moiety for Polymer Solar Cells: Contribution of the Chromophoric Substituent on C_{60} to the Photocurrent. *ACS Appl. Mater. Interfaces* **2012**, *4*, 6133−6141.
(21) Hau, S. K.; Cheng, Y.-J.; Yip, H.-L.; Zhang, Y.; Ma, H.; Jen, A. K.-Y. Effect of Chemical Modification of Fullerene-Based Self-Assembled Monolayers on the Performance of Inverted Polymer Solar Cells. *ACS Appl. Mater. Interfaces* **2010**, *2*, 1892−1902.
(22) Chen, T. L.; Zhang, Y.; Smith, P.; Tamayo, A.; Liu, Y.; Ma, B. Diketopyrrolopyrrole-Containing Oligothiophene-Fullerene Triads and Their Use in Organic Solar Cells. *ACS Appl. Mater. Interfaces* **2011**, *3*, 2275−2280.
(23) Liu, C.; Xiao, S.; Shu, X.; Li, Y.; Xu, L.; Liu, T.; Yu, Y.; Zhang, L.; Liu, H.; Li, Y. Synthesis and Photovoltaic Properties of Novel Monoadducts and Bisadducts Based on Amide Methanofullerene. *ACS Appl. Mater. Interfaces* **2012**, *4*, 1065−1071.
(24) Kang, H.; Cho, C.-H.; Cho, H.-H.; Kang, T. E.; Kim, H. J.; Kim, K.-H.; Yoon, S. C.; Kim, B. J. Controlling Number of Indene Solubilizing Groups in Multiadduct Fullerenes for Tuning Optoelectronic Properties and Open-Circuit Voltage in Organic Solar Cells. *ACS Appl. Mater. Interfaces* **2012**, *4*, 110−116.
(25) Mi, D.; Kim, J.-H.; Kim, H. U.; Xu, F.; Hwang, D.-H. Fullerene Derivatives as Electron Acceptors for Organic Photovoltaic Cells. *J. Nanosci. Nanotechnol.* **2014**, *14*, 1064−1084.
(26) Liu, H.; Xu, J.; Li, Y.; Li, Y. Aggregate Nanostructures of Organic Molecular Materials. *Acc. Chem. Res.* **2010**, *43*, 1496−1508.
(27) Liu, C.; Xu, L.; Chi, D.; Li, Y.; Liu, H.; Wang, J. Synthesis of Novel Acceptor Molecules of Mono- and Multiadduct Fullerene Derivatives for Improving Photovoltaic Performance. *ACS Appl. Mater. Interfaces* **2013**, *5*, 1061−1069.
(28) Ruderer, M. A.; Guo, S.; Meier, R.; Chiang, H.-Y.; Körstgens, V.; Wiedersich, J.; Perlich, J.; Roth, S. V.; Müller-Buschbaum, P. Solvent-Induced Morphology in Polymer-Based Systems for Organic Photovoltaics. *Adv. Funct. Mater.* **2011**, *21*, 3382−3391.
(29) Perlich, J.; Rubeck, J.; Botta, S.; Gehrke, R.; Roth, S. V.; Ruderer, M. A.; Prams, S. M.; Rawolle, M.; Zhong, Q.; Körstgens, V.; Müller-Buschbaum, P. Grazing Incidence Wide-Angle X-ray Scattering at the Wiggler Beamline BW4 of HASYLAB. *Rev. Sci. Instrum.* **2010**, *81*, 105105-1−1105105-7.
(30) Woo, C. H.; Thompson, B. C.; Kim, B. J.; Toney, M. F.; Fréchet, J. M. J. The Influence of Poly(3-hexylthiophene) Regioregularity on Fullerene-Composite Solar Cell Performance. *J. Am. Chem. Soc.* **2008**, *130*, 16324−16329.
(31) Treat, N. D.; Shuttle, C. G.; Toney, M. F.; Hawker, C. J.; Chabinyc, M. L. In Situ Measurement of Power Conversion Efficiency and Molecular Ordering During Thermal Annealing in P3HT:PCBM Bulk Heterojunction Solar Cells. *J. Mater. Chem.* **2011**, *21*, 15224−15231.
(32) Guo, S.; Ruderer, M. A.; Rawolle, M.; Körstgens, V.; Birkenstock, C.; Perlich, J.; Müller-Buschbaum, P. Evolution of Lateral Structures during the Functional Stack Build-up of P3HT:PCBM-Based Bulk Heterojunction Solar Cells. *ACS Appl. Mater. Interfaces* **2013**, *5*, 8581−8590.
(33) Fan, C.; Wang, S.; Hong, J. W.; Bazan, G. C.; Plaxco, K. W.; Heeger, A. J. Beyond Superquenching: Hyper-Efficient Energy Transfer from Conjugated Polymers to Gold Nanoparticles. *Proc. Natl. Acad. Sci. U.S.A.* **2003**, *100*, 6297−6301.
(34) Kooistra, F. B.; Knol, J.; Kastenberg, F.; Popescu, L. M.; Verhees, W. J. H.; Kroon, J. M.; Hummelen, J. C. Increasing the Open Circuit Voltage of Bulk-Heterojunction Solar Cells by Raising the LUMO Level of the Acceptor. *Org. Lett.* **2007**, *9*, 551−554.
(35) Scharber, M. C.; Mühlbacher, D.; Koppe, M.; Denk, P.; Waldauf, C.; Heeger, A. J.; Brabec, C. J. Design Rules for Donors in Bulk-Heterojunction Solar Cells-Towards 10% Energy-Conversion Efficiency. *Adv. Mater.* **2006**, *18*, 789−794.
(36) Goodman, A. M.; Rose, A. Double Extraction of Uniformly Generated Electron−Hole Pairs from Insulators with Noninjecting Contacts. *J. Appl. Phys.* **1971**, *42*, 2823−2830.
(37) Kim, K.-H.; K, H.; N, S. Y.; J, J.; Kim, P. S.; Cho, C.-H.; Lee, C.; Yoon, S. C.; Kim, B. J. Facile Synthesis of *o*-Xylenyl Fullerene Multiadducts for High Open Circuit Voltage and Efficient Polymer Solar Cells. *Chem. Mater.* **2011**, *23*, 5090−5095.
(38) Mihailetchi, V. D.; Xie, H. X.; de Boer, B.; Koster, L. J. A.; Blom, P. W. M. Charge Transport and Photocurrent Generation in Poly(3-hexylthiophene):Methanofullerene Bulk-Heterojunction Solar Cells. *Adv. Funct. Mater.* **2006**, *16*, 699−708.
(39) Blom, P. W. M.; Mihailetchi, V. D.; Koster, L. J. A.; Markov, D. E. Device Physics of Polymer:Fullerene Bulk Heterojunction Solar Cells. *Adv. Mater.* **2007**, *19*, 1551−1566.
(40) Kim, Y.; Cook, S.; Tuladhar, S. M.; Choulis, S. A.; Nelson, J.; Durrant, J. R.; Bradley, D. D. C.; Giles, M.; Mcculloch, I.; H, C.-S.; R, M. A. Strong Regioregularity Effect in Self-Organizing Conjugated Polymer Films and High-Efficiency Polythiophene:Fullerene Solar Cells. *Nat. Mater.* **2006**, *5*, 197−203.
(41) Li, G.; Shrotriya, V.; Huang, J.; Yao, Y.; Moriarty, T.; Emery, K.; Yang, Y. High-Efficiency Solution Processable Polymer Photovoltaic

Cells by Self-Organization of Polymer Blends. *Nat. Mater.* **2005**, *4*, 864−868.
(42) Schaffer, C. J.; Palumbiny, C. M.; Niedermeier, M. A.; Jendrzejewski, C.; Santoro, G.; Roth, S. V.; Müller-Buschbaum, P. A Direct Evidence of Morphological Degradation on a Nanometer Scale in Polymer Solar Cells. *Adv. Mater.* **2013**, *25*, 6760−6764.
(43) Kohn, P.; Rong, Z.; Scherer, K. H.; Sepe, A.; Sommer, M.; Müller-Buschbaum, P.; Friend, R. H.; Steiner, U.; Hüttner, S. Crystallization-Induced 10 nm Structure Formation in P3HT/PCBM Blends. *Macromolecules* **2013**, *46*, 4002−4013.
(44) Pfaff, M.; Müller, P.; Bockstaller, P.; Müller, E.; Subbiah, J.; Wong, W. W. H.; Klein, M. F. G.; Kiersnowski, A.; Puniredd, S. R.; Pisula, W.; Colsmann, A.; Gerthsen, D.; Jones, D. J. Bulk Heterojunction Nanomorphology of Fluorenyl Hexa-perihexabenzocoronene−Fullerene Blend Films. *ACS Appl. Mater. Interfaces* **2013**, *5*, 11554−11562.